Investigation of the electronic structure and lattice dynamics of the thermoelectric material Na-doped SnSe

doi: 10.1103/PhysRevB.98.094305

Investigation of the electronic structure and lattice dynamics of the thermoelectric material Na-doped SnSe

P. Wu,[1,2] B. Zhang,[1] K. L. Peng,[3] M. Hagihala,[2] Y. Ishikawa,[2] M. Kofu,[4] S. H. Lee,[2] H. Kumigashira,[5] C. S. Hu,[1] Z. M. Qi,[1] K. Nakajima,[4] G. Y. Wang,[3,*] Z. Sun,[1,6,†] and T. Kamiyama[2,‡]

[1]*National Synchrotron Radiation Laboratory, University of Science and Technology of China, Hefei, Anhui 230029, People's Republic of China*

[2]*Institute of Materials Structure Science, KEK, Tokai, Ibaraki 319-1106, Japan*

[3]*Chongqing Institute of Green and Intelligent Technology, Chinese Academy of Sciences, Chongqing 400714, People's Republic of China*

[4]*Japan Proton Accelerator Research Complex, Japan Atomic Energy Agency, Tokai, Ibaraki 319-1195, Japan*

[5]*Institute of Materials Structure Science, KEK, Tsukuba, Ibaraki 305-0801, Japan*

[6]*CAS Key Laboratory of Strongly-coupled Quantum Matter Physics, University of Science and Technology of China, Hefei, Anhui 230026, People's Republic of China*

(Received 2 April 2018; revised manuscript received 8 August 2018; published 20 September 2018)

SnSe has drawn considerable attention on a global scale due to its intrinsic low thermal conductivity and large figure of merit along the *b* axis. In Na-doped SnSe, further enhancement of the thermoelectric performance has been reported. Using angle-resolved photoemission spectroscopy and inelastic neutron scattering, we have studied how electronic structures and lattice dynamics evolve with temperature in Na-doped SnSe. Our data show that the effective mass of the Se p_z orbital along the Γ-Z direction has a very weak temperature dependence, while the chemical potential shifts significantly along with the increase in the gap size evidenced by infrared absorption measurements. Inelastic neutron scattering reveals one acoustic TA and two low-lying optical (TO1 and TO2) phonon modes. Their temperature-dependent behaviors indicate that the TO1 and TA modes contribute more to the reduction of the lattice thermal conductivity with temperature increases. The estimated value of the lattice thermal conductivity based on the lattice dynamics is significantly larger than that determined by transport measurements, suggesting that extrinsic factors, such as the imperfection of the lattice, could drastically suppress the lattice thermal conductivity. Our data suggest that temperature-dependent properties of both electronic structures and phonon dynamics need to be taken into account for the investigation of the underlying physics of hole-doped SnSe.

DOI: 10.1103/PhysRevB.98.094305

I. INTRODUCTION

The search for a sustainable supply of energy is a significant issue due to the increasing demand and the shortage of traditional sources. Thermoelectric (TE) materials are expected to provide an alternative mechanism to address the energy crisis. These are functional energy materials that enable the direct conversion of waste heat to useful electricity on the basis of the Seebeck effect. The conversion efficiency is determined by the dimensionless figure of merit $zT = S^2\sigma T/(\kappa_e + \kappa_l)$, where S, σ, κ_e, and κ_l denote the Seebeck coefficient, electrical conductivity, electrical thermal conductivity, and lattice thermal conductivity, respectively. The interdependence of these TE parameters makes it somewhat difficult to obtain an optimized zT [1]. In the previous several decades, inspired by the concept of "phonon glass, electron crystal" [2], efforts to enhance the TE performance have been focused on achieving a high power factor ($S^2\sigma$) via band convergency [3,4] or reducing the lattice thermal conductivity by means of nanostructure engineering [5,6] or searching for the intrinsic low-thermal-conductivity materials with complex structures [7] and strong lattice anharmonicity [8,9].

Recently, a record zT of 2.6 was reported in the earth-abundant and nontoxic IV-VI binary semiconductor SnSe with intrinsic ultralow thermal conductivity and a large power factor [10]. Nevertheless, the device figure of merit in pristine SnSe is merely 0.23 along its largest zT value direction, and a large potential remains for further enhancement of the TE performance in the SnSe system. Recently, Zhao *et al.* observed a significant increase in the power factor along the *b* axis from 0.27 mW m^{-1} K^{-2} in pristine SnSe to 4 mW m^{-1} K^{-2} in Na-doped SnSe at 300 K with the device figure of merit enhanced to 1.34 [11]. Meanwhile, Peng *et al.* also reported that the power factor is increased by an order of magnitude from 0.22 mW m^{-1} K^{-2} in pristine SnSe to 2.8 mW m^{-1} K^{-2} in Na-doped SnSe with the average zT improved to 1.17 [12]. The direct observation of electronic structures and collective dynamics of phonons help us to uncover the underlying thermoelectric mechanism of the zT enhancement.

The mechanism of the enhanced zT can be elucidated by virtue of angle-resolved photoemission spectroscopy (ARPES) and inelastic neutron scattering (INS), which can be used to measure the electronic structures and the lattice

*guoyuw@cigit.ac.cn
†z.sun@ustc.edu.cn
‡takashi.kamiyama@kek.jp

dynamics, respectively, in crystalline solids. These probes have revealed important properties of electrons and phonons that help us to interpret the high performance of SnSe [13–20]. However, one may notice that the performance of SnSe strongly depends on the temperatures, and the ARPES investigation has shown that the electronic structures vary significantly as a function of temperature [13,18]. These facts suggest that in order to extrapolate the thermoelectric performance over a large temperature range, we need to take into account the substantial temperature-dependent properties of electronic states and the lattice dynamics. So far, there is very limited information about how they evolve with increasing temperature.

SnSe is highly anisotropic in the electronic structures, which is believed to be responsible for the large figure of merit in this material [11]. The electronic states of the Se p_z orbital along the Γ-Z direction contribute much more spectral weight around the Fermi level than the p_y orbital along the Γ-Y direction, so the former has more influence on transport properties. Around the top of valence bands, the effective masses along different directions are highly diverse. Along the Γ-Z direction, Lu *et al.* found a drastic change in the effective mass with temperature for $T < 300$ K, which is, however, inconsistent with the corresponding band calculations [13] and the weak temperature dependence of the effective mass revealed by ARPES on the same band but along the Γ-Y direction [18]. On the other hand, ARPES measurements have shown a large shift of the chemical potential as a function of temperature, which is very important for the understanding of the physical properties of this material. There are different interpretations about its origin. For instance, it could come from the intrinsic change in band structures upon increasing temperature, or it may arise from extrinsic factors, such as sample charging in photoemission experiments [13], and the thermal excitation of holes in a hole-doped semiconductor can also result in such a large shift of the chemical potential [18]. More studies are required to reveal how the electronic structures evolve with temperature and to solve the discrepancies. Moreover, the phonon dynamics as a function of temperature can help us to gain more understanding of the lattice thermal conductivity. In particular, we can find what phonon modes contribute to the decline of the lattice thermal conductivity as temperature increases.

In the present work, ARPES and INS are used to investigate the electronic structures and lattice dynamics in Na-doped SnSe, in particular their evolutions with temperature. We find that at low temperatures the effective mass along the Γ-Z direction shows very weak temperature dependence, in contrast to previous reports by Lu *et al.* [13]. The chemical potential shifts remarkably with a trend similar to the picture of thermal excitation of hole carriers in a p-type semiconductor; meanwhile, the band gap increases with temperature. Our data suggest that the detailed electronic excitations around the Fermi level have to take into account these two factors. INS data reveal one acoustic TA and two low-lying optical (TO1 and TO2) phonon modes. Their different temperature-dependent linewidths indicate that the TO1 and TA modes contribute more significantly to the reduction of the lattice thermal conductivity with increasing temperature. We also estimate the lattice thermal conductivity based on the lattice dynamics, which is significantly larger than the value from transport measurements, suggesting that extrinsic ingredients, such as the imperfection of lattice, could play an important role in the suppression of the lattice thermal conductivity. Our findings suggest that the detailed temperature-dependent behavior of electronic structures and phonon dynamics have to be considered to quantitatively account for the underlying physics of hole-doped SnSe.

II. EXPERIMENTAL METHODS

A high-quality single crystal of Na-doped SnSe was fabricated using a modified Bridgman method, and the growth direction of the single-crystal rod was determined by the electron backscattered diffraction analysis using scanning electron microscopy (JEOL JSM-7800F) [21]. ARPES measurements were conducted at BL-13U of the National Synchrotron Radiation Laboratory (NSRL) at Hefei, which was equipped with a VG-Scienta R4000 hemispherical analyzer. The overall energy resolution was better than 30 meV, and the angular resolution was 0.3°. The flat and shiny surfaces were obtained through *in situ* cleavage under a vacuum pressure that was better than 6×10^{-11} mbar at $T = 20$ K. The core-level photoemission spectrum was collected at BL-28 of the Photon Factory at Japan's National Laboratory for High Energy Physics using an SES 2002 hemispherical electron analyzer. The Fermi level of the samples was referenced using polycrystalline gold that was evaporated onto the sample holder. Temperature-dependent neutron powder diffraction (NPD) data were collected at BL-09 SPICA of the Materials and Life Science Experimental Facility in the Japan Proton Accelerator Research Complex (J-PARC). A single crystal with a weight of 3.2 g was ground into powder and was sealed into a vanadium can. The NPD data were analyzed using the Z-RIETVELD software [22]. High-resolution INS measurements were carried out using a time-of-flight chopper spectrometer at BL-14 AMATERAS in J-PARC [23]. A single crystal with a weight of 8.4 g was mounted onto the closed-cycle He refrigerator sample holder with the b-c plane in a direction parallel to the incident neutron beam. The four-dimensional experimental data were reduced and visualized using the UTSUSEMI software [24]. Infrared absorption experiments were carried out at the BL-01B of NSRL using a Bruker Vertex 70V FT-IR spectrometer.

III. RESULTS AND DISCUSSIONS

The crystal structure of Na-doped SnSe is illustrated in Fig. 1(a), possessing the layered stacked structure with the Sn-Se chains corrugated along the c axis, and the corresponding Brillouin zone is shown in Fig. 1(b). Figure 1(c) shows the core-level x-ray photoemission spectrum of Na-doped SnSe. The sharp characteristic peaks indicate the high quality of the samples. The tiny amount of Na content can be identified by zooming in on the spectrum as shown in the inset. Figures 1(d) and 1(e) show the NPD patterns collected at 15 and 410 K, respectively. A good fit of R_{wp} was achieved, yielding values of 3.58% and 3.50% for 15 and 410 K, respectively. The occupancy of Se is refined to be 0.99343(9), suggesting a

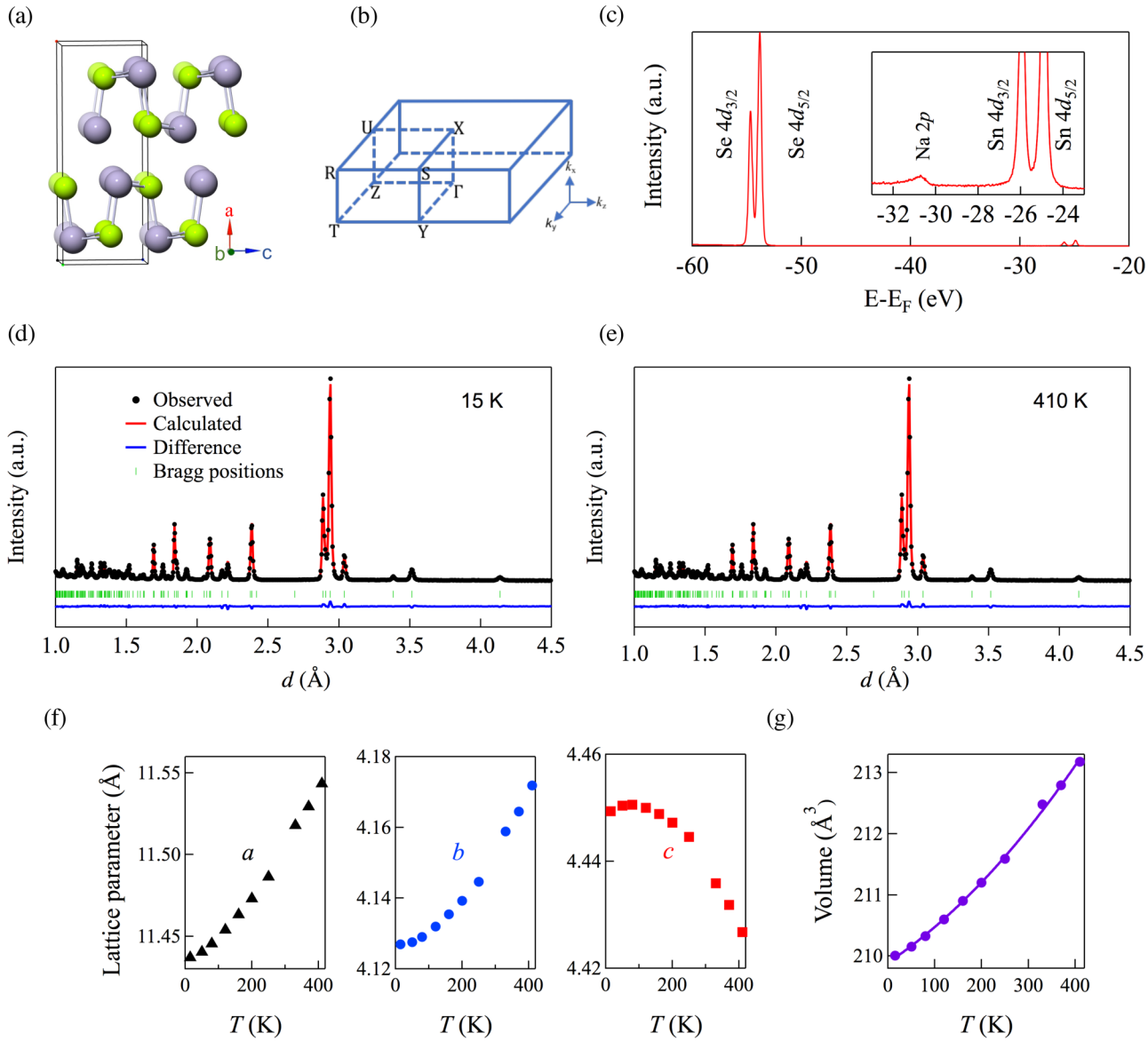

FIG. 1. (a) The crystal structure of Na-doped SnSe in the *Pnma* phase; here, Sn(Na) and Se atoms are represented by the gray and green balls, respectively. (b) The Brillouin zone of Na-doped SnSe with high-symmetry points. (c) The core-level photoemission spectrum of Na-doped SnSe; the Na 2*p* and Sn 4*d* characteristic peaks are illustrated in the inset. (d) and (e) Rietveld refinement of neutron powder diffraction data collected at 15 and 410 K, respectively. The black dots represent the observed results. The red and blue lines correspond to the calculated and difference patterns, respectively. The green ticks are the Bragg positions. (f) Temperature dependence of the lattice constants *a*, *b*, and *c*, derived from the Rietveld refinements of the neutron power diffraction patterns. (g) The volume of Na-doped SnSe as a function of temperature. The solid line is the parabolic fitting of the volume.

minute deviation from the stoichiometry occupancy. Sodium occupies the Sn site with an occupancy of 0.0197(3), which is less than the nominal doping value of 0.03. This discrepancy arises from the fact that, during the synthesis procedure, the sodium element can escape from the crystal, which leads to a loss of Na concentration. Na dopants play the role of hole doping, while Se deficiency acts in the manner of electron doping. With both taken into account, a hole carrier concentration of 1.2×10^{20} cm^{-3} can be derived from our neutron power diffraction refinement, which is comparable to the value of 9×10^{19} cm^{-3} at room temperature obtained from the Hall measurement [12]. Figure 1(f) depicts the temperature dependence of the lattice constants determined by the Rietveld refinements of the neutron powder diffraction patterns. The lattice constants *a* and *b* display a positive thermal expansion, whereas lattice constant *c* exhibits a negative thermal expansion. It is known that SnSe undergoes a structural phase transition from the *Pnma* to *Cmcm* space group at 807 K [25]. Upon increasing the temperature, a decrease in the degree of the corrugation of Sn-Se bilayers occurs [26]. Figure 1(g) illustrates the volume of Na-doped SnSe as a function of temperature, with a volume thermal expansion coefficient α of $2.41 \times 10^{-5} + 7.11 \times 10^{-8}\ T$ derived using a parabolic fitting.

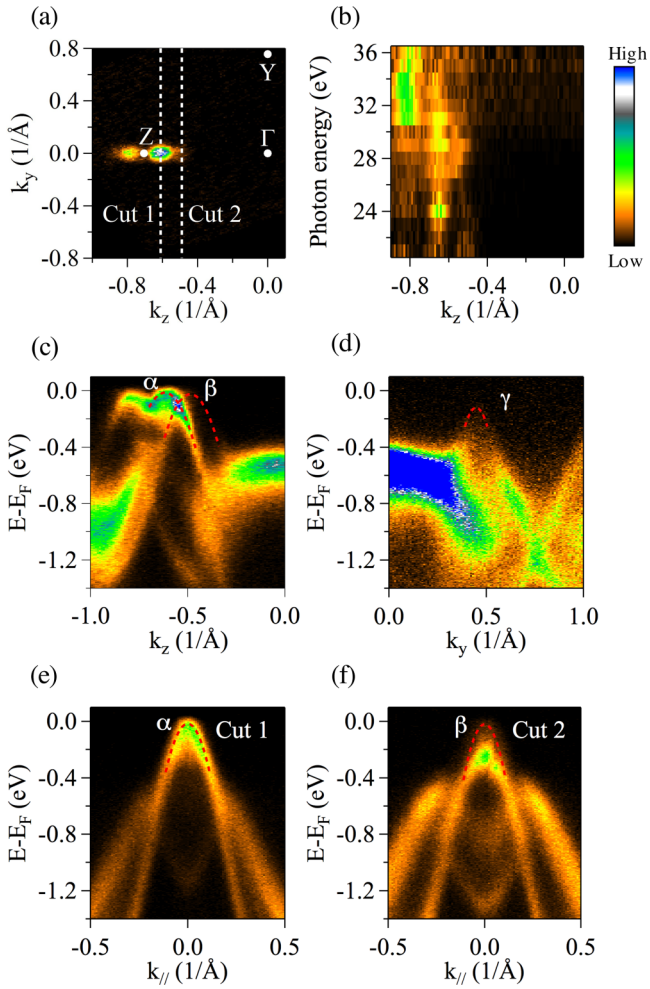

FIG. 2. (a) Fermi surface mapping of the k_y-k_z plane using the incident photon energy of 30 eV at $T = 20$ K. (b) The photon energy dependence plot of the photoemission intensity at the Fermi level along the Γ-Z direction taken at $T = 20$ K. (c) and (d) The ARPES intensity plot along the Γ-Z and Γ-Y directions, respectively. (e) and (f) The ARPES intensity distribution along cuts 1 and 2, respectively, in (a). The red dashed lines in (c)–(f) indicate the dispersions around the tops of these bands, which can approximately evaluate the effective masses.

Figure 2(a) presents the ARPES intensity of the k_y-k_z plane at the Fermi level. The Fermi surface comprises four ellipsoidal pockets along the Z-Γ-Z direction, which is in accordance with the metallic characteristic of Na-doped SnSe that was observed in the transport measurement [12]. The intensity of the ellipsoidal pocket that lies at the momentum of $k_z = -0.5$ Å^{-1} is observed to be very weak even though its feature can be resolved by examining the data carefully. In contrast to the Z-Γ-Z direction, the Fermi pockets are absent along the Y-Γ-Y direction, with the electronic band top lying below the Fermi level, indicating the anisotropic electronic structures of Na-doped SnSe. Such band structures are consistent with previous reports on both pristine SnSe and the hole-doped compound [13–19]. To investigate the dimensionality of the ellipsoidal pockets, we varied photon energies from 21 to 36 eV with a 1 eV step to map the spectral weight at the Fermi level along the Z-Γ-Z direction [see Fig. 2(b)]. The electronic states at $k_z = -0.5$ Å^{-1} and ~ -0.6 Å^{-1}, which correspond to the pockets in Fig. 2(a), show very weak variations as a function of photon energy. This suggests the quasi-two-dimensionality of the electronic states of Na-doped SnSe, in agreement with previous studies [14,17,19].

The ARPES intensity plot along the Γ-Z direction is displayed in Fig. 2(c). The maxima of the α and β bands are observed to be in the vicinity of the Fermi level. The valleylike bands of α and β result in a band convergence of the four in one Brillouin zone. Pristine SnSe exhibits semiconductor characteristics with the band top located at 0.3 eV below the Fermi level [17]. Through sodium doping, the Fermi level was shifted down to the bending points (band maximum) of the α and β bands. Figure 2(d) shows the low-lying electronic structures along the Γ-Y direction. A very steep dispersion (labeled γ) is observed with the band top well below the Fermi level. By fitting the parabolic function to the band tops, the effective masses of $0.24m_e$, $0.22m_e$, and $0.09m_e$ were deduced for the α, β, and γ bands, respectively. Figures 2(e) and 2(f) show ARPES cuts taken along cuts 1 and 2, respectively, as indicated in Fig. 2(a). Effective masses of $0.14m_e$ and $0.12m_e$ were extracted for the α and β bands, respectively, which are about 50% of the values along the Γ-Z direction. This finding is partially accountable for the anisotropy of the electronic structures, which is in agreement with previous studies on SnSe and Na-doped SnSe [14,17,19]. From the electronic structures revealed by ARPES, we can identify four maxima of valence bands in the vicinity of the Fermi level along the Z-Γ-Z direction, which gives rise to the enlargement of the electrical conductivity and thus the enhancement of the power factor. The anisotropy parameters (defined as m_z/m_y) are 1.7 and 1.9 for the α and β bands, respectively. Such large band convergence and anisotropy of the electronic bands are responsible for the large figure of merit in Na-doped SnSe.

To elucidate the evolution of the electron structures with temperature, we performed temperature-dependent ARPES measurements. Figures 3(a) and 3(b) illustrate the ARPES intensity plots along the Γ-Z direction at $T = 60$ and 240 K, respectively. The valleylike bands exhibit a distinct shift towards higher binding energy at 240 K. This observation is in line with recent ARPES works [13,18]. By fitting the dispersion of the band top of the α band with a parabolic curve, an effective mass of $0.21m_e$ is derived at 240 K. This indicates that the effective mass of the carrier does not show substantial variations as a function of temperature. This result is in accordance with the weak temperature-dependent behavior of the effective mass along the Γ-Y direction of the α band [18], which is, however, inconsistent with the significant reduction of the effective mass observed by Lu *et al.* [13]. According to the density functional theory calculations by Lu *et al.* [13], the effective masses exhibit nearly constant values in the low-T *Pnma* phase [13], which is also in good agreement with our results. The weak change in effective masses can also be evidenced by comparing the band structures in Figs. 3(a) and 3(b), in which the overall band dispersions remain basically the same from 60 to 240 K, although they move to deeper binding energies with increasing temperature. Figure 3(c)

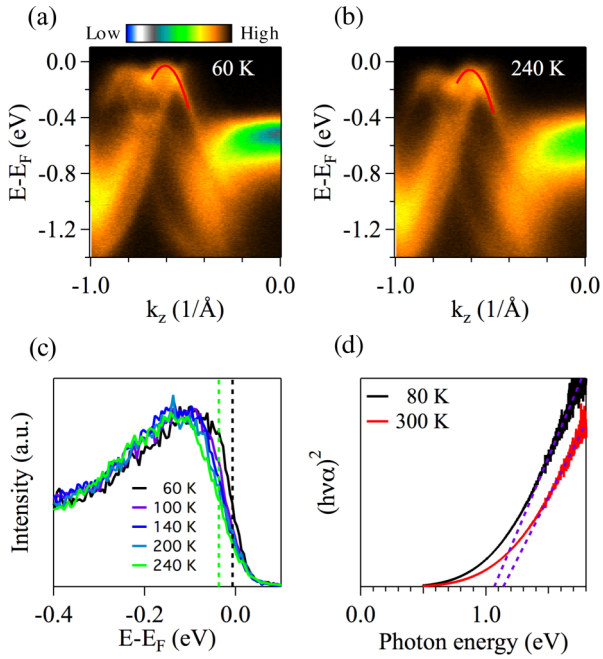

FIG. 3. Temperature dependence of the ARPES intensity along the Γ-Z direction. (a) and (b) The electronic structures along the Γ-Z direction that were observed at an incident photon energy of 30 eV at $T = 60$ and 240 K, respectively. (c) Temperature-dependent energy distribution curves integrated over a momentum window of 0.03 Å^{-1} centered around the top of the α band. (d) Infrared absorption data plotted as $(\alpha h\nu)^2$ versus photon energy to show the variation of the direct band gap with temperature.

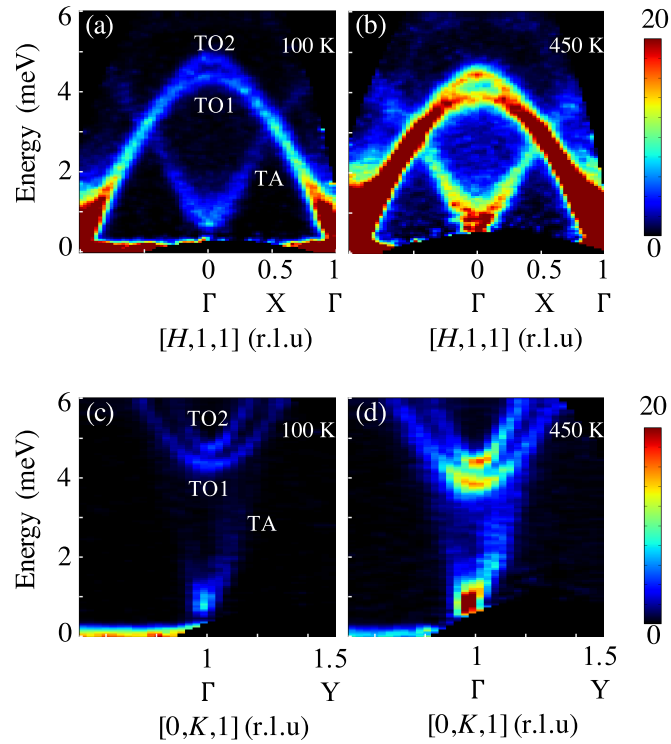

FIG. 4. Phonon dispersions of Na-doped SnSe using the incident neutron energy of 7.74 meV. (a) and (c) The phonon dispersions along the $[H, 1, 1]$ and $[0, K, 1]$ directions, respectively. The data were taken at $T = 100$ K. (b) and (d) The same as (a) and (c), but taken at $T = 450$ K. The lower and upper transverse optical modes are labeled as TO1 and TO2, respectively.

shows the temperature dependence of the energy distribution curves (EDCs) integrated over a window of 0.03 Å^{-1} with respect to the top of the α band. Using the EDC leading edge as a reference, they have also clearly shown that the valence band moves towards higher binding energy by ∼30 meV with increasing the temperature from 60 to 240 K. This energy shift also corresponds to a chemical potential shift. In order to quantitatively estimate the Seebeck coefficient from the shift of the chemical potential, we have adopted the formula proposed by Yamamoto *et al.* [27],

$$S(T) \approx \frac{T[\mu(T) - \mu(T_1)]}{e\left(T^2 - T_1^2\right)},$$

where μ is the chemical potential. From 60 to 240 K, the chemical potential shift is ∼30 meV, yielding a Seebeck coefficient of 0.133 mV K^{-1}, which is close to the value of 0.116 mV K^{-1} at 280 K derived from ARPES data [18] and the reported value of 0.16 mV K^{-1} at 300 K from transport measurements [11,12].

We have performed infrared absorption measurements to examine whether the electronic structures across the band gap vary with increasing temperature in Na-doped SnSe. Our data show that the direct gap size varies from 1.07 to 1.14 eV when the temperature changes from 80 to 300 K. This variation of the gap size demonstrates the intrinsic change in electronic structures around the top of the valence bands and the bottom of the conduction bands. Generally speaking, the chemical potential of a semiconductor at a specific temperature is determined by the carrier concentration and the thermal excitation of carriers at that temperature; the effects of these two factors, however, are also intertwined with the fine electronic structures around the top of the valence bands and the bottom of the conduction bands. Therefore, we argue that the large chemical potential shift in the Na-doped SnSe (which is also related to the shift of valence bands) is mainly dominated by the thermal excitation of holes, while the temperature-dependent variation of intrinsic electronic structures around the top of the valence bands should also be taken into account for a comprehensive understanding of the unusual large shift of the valence bands.

Next, we turn our attention to the phonon dynamics. Figures 4(a) and 4(b) show the two-dimensional neutron intensity distribution along the $[H, 1, 1]$ direction using an incident neutron energy of 7.74 meV at $T = 100$ and 450 K, respectively. The TO branch crosses the TA branch at an energy transfer of ∼3 meV at the zone boundary. Similar to the case that is observed in the $[H, 1, 1]$ direction, the TA phonons propagating along the $[0, K, 1]$ direction also display an evident overlap with the TO phonons at an energy transfer of ∼4.5 meV [see Figs. 4(c) and 4(d)]. It is worth mentioning that two optical modes (labeled TO1 and TO2, respectively) with wide energy degeneracy are clearly resolved by INS. According to the previous study on pristine SnSe, the TO1 and TO2 modes correspond to the c and b polarized modes,

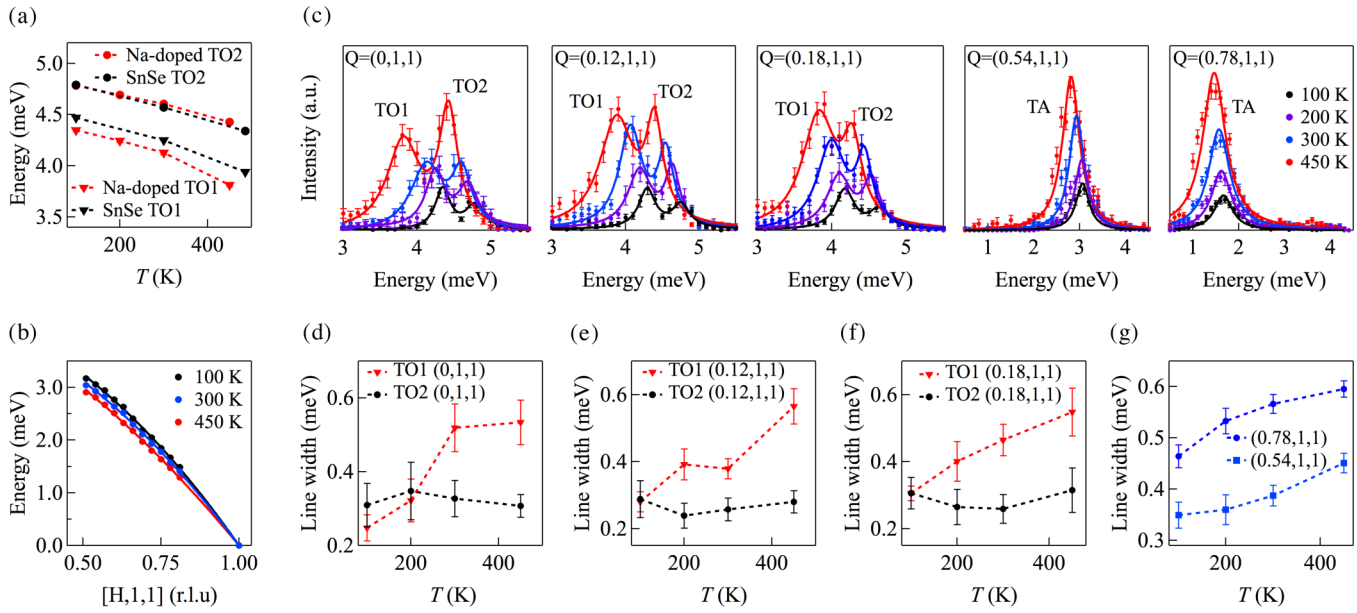

FIG. 5. Transverse acoustic and optical phonon modes along the $[H, 1, 1]$ direction. (a) The comparison of the low-lying TO modes between the pristine and Na-doped SnSe. The red symbols are derived from the Na-doped SnSe, and the black symbols are from the pristine SnSe [20]. (b) The dispersion relationship of the TA phonon at $T = 100$, 300, and 450 K. The solid lines correspond to the parabolic curve fitting. (c) Lorentzian fittings of spectra for Na-doped SnSe for different wave vectors. (d)–(f) Temperature dependence of the experimental phonon linewidth of the low-lying TO branches at $Q = [0, 1, 1]$, [0.12,1,1], and [0.18,1,1], respectively. (g) Temperature dependence of the experimental phonon linewidth of the TA branch at $Q = [0.54, 1, 1]$ and [0.78,1,1].

respectively, and they have also been observed at zone centers [0,1,2] and [0,0,2] [20].

Figure 5 demonstrates the evolution of the phonon modes with temperature along the $[H, 1, 1]$ direction in Na-doped SnSe. In Fig. 5(a), the phonon modes at the zone center of Na-doped SnSe exhibit noticeable softening with increasing temperature, showing the same trend as the case of the pristine SnSe [20]. Compared to the pristine SnSe, the TO1 phonon of the Na-doped SnSe at the zone center exhibits a 0.12 meV softening in the measured temperature range. Likewise, the softening of the TA phonon can also be clearly observed in Fig. 5(b). By fitting the parabolic curve to the TA branch, velocities of 2342(32) and 2000(25) m s^{-1} are derived at 100 and 450 K, respectively. In the framework of the relaxation time approximation, the lattice thermal conductivity can be determined by $\kappa_l = 1/3 c_V \langle V(q)^2 \tau(q) \rangle$, where c_V is the heat capacity and $V(q)$ and $\tau(q)$ are the phonon group velocity and lifetime at a specified wave vector, respectively. At $T = 300$ K, c_V is 1.2 J cm^{-3} K^{-1} [28], and $\langle V(q)^2 \tau(q) \rangle$ is estimated to be 6.6×10^{-6} m^2 s^{-1} for the TA branch along the $[H, 1, 1]$ direction. Accordingly, the lattice thermal conductivity from the TA mode is estimated to be 2.6 W m^{-1} K^{-1}. Owing to the factor of the instrumental resolution, this value actually underestimates the value of intrinsic lattice thermal conductivity. However, the estimated value from INS data is significantly larger than the number derived from the transport measurements (0.45 W m^{-1} K^{-1} at 300 K) [11]. This remarkable discrepancy suggests that some imperfection of the lattice, such as grain boundaries or deficiencies [29], could significantly suppress the lattice thermal conductivity.

The Lorentzian fittings of the spectra at different momentum transfers are illustrated in Fig. 5(c); in particular, one can notice that TO1 and TO2 phonon modes can be well resolved throughout the whole temperature range in our study. Figures 5(d)–5(g) show the temperature dependence of the experimental phonon linewidth. A decline in thermal conductivity can be induced by phonon-phonon scattering, which becomes stronger with increasing temperature and is manifested in a manner of linewidth broadening. Taking advantage of the high-resolution data, we investigated the temperature-dependent linewidth of the low-lying phonons. We found that the linewidth of TO1 and TA phonons along the $[H, 1, 1]$ direction shows significant broadening with increasing temperature, while the linewidth of the TO2 phonon has a very weak temperature-dependent behavior. Our result reveals that TA and TO1 phonon modes contribute more to the decline of the lattice thermal conductivity as temperature increases, while the TO2 phonon does not. These details help us to achieve a better understanding of the lattice dynamics of SnSe.

IV. CONCLUSIONS

In summary, we have studied how electronic structures and phonon dynamics evolve with temperatures in Na-doped SnSe. Our data indicate that the effective mass has a weak temperature dependence along the Γ-Z direction at low temperatures, in contrast to the reports by Lu *et al.* [13]. The significant shift of the chemical potential with temperature is associated with the thermal excitations of holes in this hole-doped material. However, the increase of the band gap with temperature indicates that the change in electronic structures around the top of the valence bands and the bottom of the conduction bands also needs to be taken into account to

quantitatively depict electronic properties around the Fermi level. The INS data reveal that the low-lying TO1 and TA phonon modes contribute to the decline of the lattice thermal conductivity with increasing temperatures, while the TO2 mode does not. Moreover, our INS data suggest that extrinsic factors, such as deficiencies or grain boundaries, have a strong effect on the reduction of the lattice thermal conductivity, which could effectively improve the performance of the TE in Na-doped SnSe. Our findings provide valuable information for a better understanding of the high performance of Na-doped SnSe, which could be helpful for the further enhancement of zT in SnSe. In particular, the remarkable variations of electronic structures and phonon dynamics with temperature suggest that it is inadequate to extrapolate the thermoelectric performance by merely adopting the low-temperature band structures or phonon dynamics as the input parameters, and their evolution with temperature has to be further investigated to quantitatively account for the high performance of hole-doped SnSe.

ACKNOWLEDGMENTS

We appreciate the assistance from T. Masuda with the single-crystal alignment by Laue diffraction. P.W. acknowledges the financial support that was provided by the China Scholarship Council. This work is supported by the National Natural Science Foundation of China (Grants No. 51472036 and No. U1532136), National Key R&D Program of China (Grant No. 2017YFA0402901), Key Research Program of Frontier Sciences, CAS (Grant No. QYZDB-SSW-SLH016), TIA-Kakehashi (Grant No. TK17-52), J-PARC (Proposals No. 2017A0198 and No. 2017A0218), and KEK-PF (Proposal No. 2017PF-01).

P.W. and B.Z. contributed equally.

[1] T. Zhu, Y. Liu, C. Fu, J. P. Heremans, J. G. Snyder, and X. Zhao, Adv. Mater. **29**, 1605884 (2017).

[2] D. M. Rowe, *CRC Handbook of Thermoelectrics* (CRC Press, Boca Raton, FL, 1995).

[3] W. Liu, X. Tan, K. Yin, H. Liu, X. Tang, J. Shi, Q. Zhang, and C. Uher, Phys. Rev. Lett. **108**, 166601 (2012).

[4] Y. Pei, X. Shi, A. LaLonde, H. Wang, L. Chen, and G. J. Snyder, Nature (London) **473**, 66 (2011).

[5] M. G. Kanatzidis, Chem. Mater. **22**, 648 (2009).

[6] B. Poudel, Q. Hao, Y. Ma, Y. Lan, A. Minnich, B. Yu, X. Yan, D. Wang, A. Muto, D. Vashaee, X. Chen, J. Liu, M. S. Dresselhaus, G. Chen, and Z. Ren, Science **320**, 634 (2008).

[7] T. Takabatake, K. Suekuni, T. Nakayama, and E. Kaneshita, Rev. Mod. Phys. **86**, 669 (2014).

[8] C. W. Li, J. Ma, H. B. Cao, A. F. May, D. L. Abernathy, G. Ehlers, C. Hoffmann, X. Wang, T. Hong, A. Huq, O. Gourdon, and O. Delaire, Phys. Rev. B **90**, 214303 (2014).

[9] D.-T. Morelli, V. Jovovic, and J.-P. Heremans, Phys. Rev. Lett. **101**, 035901 (2008).

[10] L.-D. Zhao, S.-H. Lo, Y. Zhang, H. Sun, G. Tan, C. Uher, C. Wolverton, V. P. Dravid, and M. G. Kanatzidis, Nature (London) **508**, 373 (2014).

[11] L.-D. Zhao, G. Tan, S. Hao, J. He, Y. Pei, H. Chi, H. Wang, S. Gong, H. Xu, V. P. Dravid, C. Uher, G. J. Snyder, C. Wolverton, and M. G. Kanatzidis, Science **351**, 141 (2016).

[12] K. Peng, X. Lu, H. Zhan, S. Hui, X. Tang, G. Wang, J. Dai, C. Uher, G. Wang, and X. Zhou, Energy Environ. Sci. **9**, 454 (2016).

[13] Q. Lu, M. Wu, D. Wu, C. Chang, Y.-P. Guo, C.-S. Zhou, W. Li, X.-M. Ma, G. Wang, L.-D. Zhao, L. Huang, C. Liu, and J. He, Phys. Rev. Lett. **119**, 116401 (2017).

[14] C. W. Wang, Y. Y. Y. Xia, Z. Tian, J. Jiang, B. H. Li, S. T. Cui, H. F. Yang, A. J. Liang, X. Y. Zhan, G. H. Hong, S. Liu, C. Chen, M. X. Wang, L. X. Yang, Z. Liu, Q. X. Mi, G. Li, J. M. Xue, Z. K. Liu, and Y. L. Chen, Phys. Rev. B **96**, 165118 (2017).

[15] T. Nagayama, K. Terashima, T. Wakita, H. Fujiwara, T. Fukura, Y. Yano, K. Ono, H. Kumigashira, O. Ogiso, A. Yamashita, Y. Takano, H. Mori, H. Usui, M. Ochi, K. Kuroki, Y. Muraoka, and T. Yokoya, Jpn. J. Appl. Phys. **57**, 010301 (2017).

[16] Z. Wang, C. Fan, Z. Shen, C. Hua, Q. Hu, F. Sheng, Y. Lu, H. Fang, Z. Qiu, J. Lu, Z. Liu, W. Liu, Y. Huang, Z.-A. Xu, D. W. Shen, and Y. Zheng, Nat. Commun. **9**, 47 (2018).

[17] V. Tayari, B. V. Senkovskiy, D. Rybkovskiy, N. Ehlen, A. Fedorov, C.-Y. Chen, J. Avila, M. Asensio, A. Perucchi, P. di Pietro, L. Yashina, I. Fakih, N. Hemsworth, M. Petrescu, G. Gervais, A. Grüneis, and T. Szkopek, Phys. Rev. B **97**, 045424 (2018).

[18] M. Maeda, K. Yamamoto, T. Mizokawa, N. L. Saini, M. Arita, H. Namatame, M. Taniguchi, G. Tan, L. D. Zhao, and M. G. Kanatzidis, Phys. Rev. B **97**, 121110(R) (2018).

[19] I. Pletikosić, F. von Rohr, P. Pervan, P. K. Das, I. Vobornik, R. J. Cava, and T. Valla, Phys. Rev. Lett. **120**, 156403 (2018).

[20] C. W. Li, J. Hong, A. F. May, D. Bansal, S. Chi, T. Hong, G. Ehlers, and O. Delaire, Nat. Phys. **11**, 1063 (2015).

[21] K. Peng, B. Zhang, H. Wu, X. Cao, A. Li, D. Yang, X. Lu, G. Wang, X. Han, C. Uher, and X. Zhou, Mater. Today **21**, 501 (2018).

[22] R. Oishi, M. Yonemura, Y. Nishimaki, S. Torii, A. Hoshikawa, T. Ishigaki, T. Morishima, K. Mori, and T. Kamiyama, Nucl. Instrum. Methods Phys. Res., Sect. A **600**, 94 (2009).

[23] K. Nakajima, S. Ohira-Kawamura, T. Kikuchi, M. Nakamura, R. Kajimoto, Y. Inamura, N. Takahashi, K. Aizawa, K. Suzuya, K. Shibata *et al.*, J. Phys. Soc. Jpn. **80**, SB028 (2011).

[24] Y. Inamura, T. Nakatani, J. Suzuki, and T. Otomo, J. Phys. Soc. Jpn. **82**, SA031 (2013).

[25] T. Chattopadhyay, J. Pannetier, and H. Von Schnering, J. Phys. Chem. Solids **47**, 879 (1986).

[26] D. Bansal, J. Hong, C. W. Li, A. F. May, W. Porter, M. Y. Hu, D. L. Abernathy, and O. Delaire, Phys. Rev. B **94**, 054307 (2016).

[27] A. Yamamoto, K. Ogawa, and T. Takeuchi, Mater. Trans. **52**, 1539 (2011).

[28] Y. Xiao, C. Chang, Y. Pei, D. Wu, K. Peng, X. Zhou, S. Gong, J. He, Y. Zhang, Z. Zeng *et al.*, Phys. Rev. B **94**, 125203 (2016).

[29] Z.-G. Chen, X. Shi, L.-D. Zhao, and J. Zou, Prog. Mater. Sci. **97**, 283 (2018).